European Conference on Computational Fluid Dynamics
ECCOMAS CFD 2006
P. Wesseling, E. Oñate and J. Périaux (Eds)

NUMERICAL SIMULATIONS OF THERMALLY STRATIFIED FLOWS IN AN OPEN DOMAIN

T. Dubois*, R. Touzani**

Laboratoire de Mathématiques,
Université Blaise Pascal and CNRS, 63177 Aubière, France
*e-mail: Thierry.Dubois@math.univ-bpclermont.fr
web page: http://math.univ-bpclermont.fr/~thdubois
**e-mail: Rachid.Touzani@math.univ-bpclermont.fr
web page: http://math.univ-bpclermont.fr/~touzani

Key words: Boussinesq equations, incompressible flows, natural convection, finite difference scheme, open domain, heat island circulation

Abstract. *We present two dimensional numerical simulations of circulation induced by a heat island in an unbounded domain. The flow is thermally stratified in the vertical direction. Boussinesq equations in a closed domain are used to describe the flow variables. For this problem, very elongated computational domains have to be used in order to obtain accurate solutions. A term, whose effect is to smoothly damp the convective terms in a layer close to the vertical boundaries, is introduced in the temperature equation. Therefore, shorter domains can be considered. This method is investigated through the numerical simulations of stationary solutions at Rayleigh number* $Ra = 10^5$ *and* 2.5×10^5*. Time periodic solutions at* $Ra = 5 \times 10^5$ *and* 10^6 *are also reported and analyzed.*

1 INTRODUCTION

In this paper we present numerical simulations of a particular type of thermal fluid flow. Namely, we are concerned with the so-called *heat island* flows[1], *i.e.* fluid flows where natural convection is generated by a local variation of temperature thus inducing Buoyancy effect. This phenomenon is generally created in the presence of heat stratification that stabilizes the fluid flow. The present model is generally used to study environment problem such as urban heat island[1].

For this problem, the flow circulation mainly occurs in an area surrounding the heat island. The combined effects of the gravity force and of the vertical stratification tend to push the flow down to the ground. Simultaneously, the heat island perturbation generates an ascending flow circulation. As a consequence of these opposite forces, thermal perturbations are propagated in the horizontal direction at long distance far from the heated element. Therefore, very elongated domains have to be used in order to accurately compute the temperature deviation from the stratified profile. Despite the increase of

computational resources, the direct simulation of such flows in *large* domains remains a real challenge. In order to reduce the size of the computational domain, a modified temperature equation is proposed here: convective terms are *smoothly* reduced with respect to the horizontal distance from the heat island in an area close to the domain boundaries.

In the next section, the physical problem and the set of equations that govern the fluid flow are described. The equations are written in non dimensional form so that the system depends on two parameters: the Rayleigh number and the vertical stratification parameter. The Section 3 is devoted to the numerical approximation. The time discretization is achieved with a second-order projection scheme to solve the velocity and pressure from which the computation of the potential temperature is decoupled. Second-order centered finite difference on a staggered grid are applied for the space discretization. The use of a centered scheme to discretize the nonlinear term coupled with a projection method provides a kinetic energy conservative scheme in the absence of viscous terms in the Navier-Stokes equation. Therefore, no artificial diffusion is introduced in the discretized system. Then, a truncated temperature equation, whose aim is to reduce the length of the computational domain, is described. The efficiency of this procedure is shown through the numerical simulation of the stationary solution at Rayleigh number $\mathrm{Ra} = 10^5$ and for a spatial resolution $h = 1/32$. At $\mathrm{Ra} = 2.5 \times 10^5$ a stationary solution is computed while time periodic solutions are obtained at $\mathrm{Ra} = 5 \times 10^5$ and $\mathrm{Ra} = 10^6$. These results reported and analyzed in the last section are preliminary results for the heat island problem considered in this paper.

2 THE SETTING OF THE PROBLEM

2.1 Description of the physical problem

We consider a fluid in the half plane $\{\mathbf{x}^\star = (x^\star, y^\star) \in \mathbb{R}^2; y^\star > 0\}$. Here and in the sequel the superscript * is used to denote physical variables. The fluid is initially at rest and is thermally stratified in the vertical direction, namely

$$\mathbf{u}^\star = \mathbf{0} \ \text{ and } \ T^\star = T_0 + \alpha_{\mathrm{s}}\, y^\star \text{ at } t = 0, \tag{1}$$

where $T_0 > 0$ is the potential temperature at the ground and $\alpha_{\mathrm{s}} > 0$ is the thermal stratification coefficient. A constant and uniform temperature $T_1 > 0$ is applied on a source-line $Q^\star = (-\delta/2, \delta/2)$ on the horizontal axis (see Figure 1).

This local thermal perturbation generates under convective effects a thermal plume. The combined effects of the gravity force and of the vertical stratification limit the development of flow structures in the vertical direction. Therefore, it seems reasonable to bound from above the region where the fluid flow is studied. A constant temperature deduced from (1) is applied at the top boundary. The heat island perturbation induces an ascending flow circulation. As a consequence of these opposite forces, thermal perturbations are propagated in the horizontal direction at long distance far from the heated element. We choose hereafter to handle this difficulty by using bounded computational

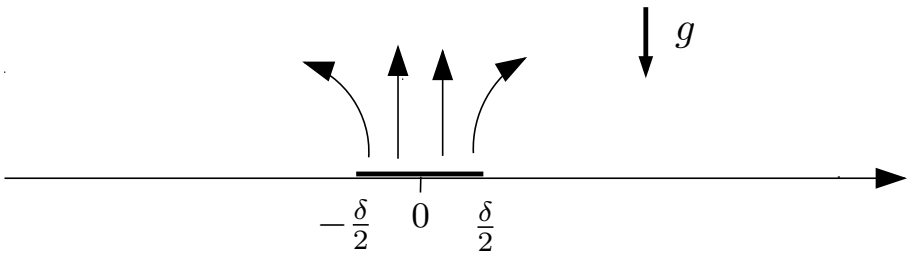

Figure 1: Heat island perturbation

domains which are *very* elongated in the horizontal direction. An appropriate design of the behaviour of the solution close to these boundaries is proposed in Section 3.

2.2 The governing equations

We consider a flow in a two dimensional bounded domain $\Omega^\star = (-L^\star/2, L^\star/2) \times (0, H^\star)$ described by the Navier-Stokes equations under the Boussinesq approximation, as shown on Figure 2. Velocity $\mathbf{u}^\star = (u^\star, v^\star)$, pressure $p^\star$, density $\rho^\star$ and potential temperature $T^\star$ satisfy:

$$\frac{\partial \mathbf{u}^\star}{\partial t} - \nu\, \Delta \mathbf{u}^\star + \nabla \cdot (\mathbf{u}^\star \otimes \mathbf{u}^\star) + \frac{\nabla p^\star}{\rho_0} \;=\; -\frac{\rho^\star}{\rho_0}\, g\, \mathbf{e}_2, \tag{2}$$

$$\nabla \cdot \mathbf{u}^\star = 0, \tag{3}$$

$$\frac{\partial T^\star}{\partial t} - \kappa\, \Delta T^\star + \nabla \cdot (\mathbf{u}^\star\, T^\star) \;=\; 0, \tag{4}$$

$$\mathbf{u}^\star(\mathbf{x}, t = 0) \;=\; \mathbf{0},\; T^\star(\mathbf{x}, t = 0) \;=\; T_0^\star(\mathbf{x}), \tag{5}$$

where ν is the kinematic viscosity, κ is the thermal conductivity and g is the gravity acceleration. In (2), $\mathbf{e}_2$ denotes the unit vector of coordinates $(0, 1)$.

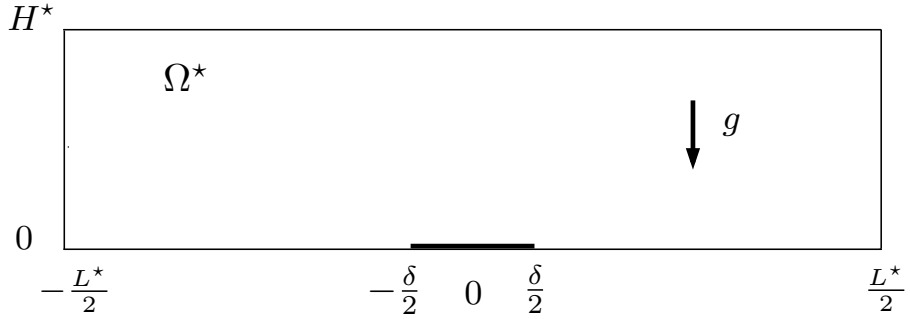

Figure 2: Computational domain

For these type of flows, the effect of pressure fluctuations on density are neglected. Compressibility is expressed in terms of the temperature variations, with respect to a

reference state (T_0, ρ_0), by a dilation equation

$$\rho^\star \,=\, \rho_0\,(1-\beta\,(T^\star - T_0)), \tag{6}$$

where β is a thermal expansion coefficient. The system (2)-(6) is supplemented with boundary conditions namely, for all $t^\star > 0$, we have

$$\mathbf{u}^\star(\mathbf{x}^\star, t^\star) \,=\, \mathbf{0} \qquad \text{on} \;\; \Gamma^\star = \partial\Omega^\star, \tag{7}$$

$$T^\star(\mathbf{x}^\star, t^\star) \,=\, T_0 + \alpha_{\rm s}\, y^\star \quad \text{on} \;\; \Gamma^\star, \tag{8}$$

$$T^\star(\mathbf{x}^\star, t^\star) \,=\, T_0 + T_1 \qquad \text{on} \;\; \Gamma^\star_Q = \{\mathbf{x}^\star \in \Gamma^\star;\, y^\star = 0,\, x^\star \in Q^\star\}, \tag{9}$$

where $T_1 > 0$ is the temperature of the heat island. These boundary conditions are acceptable only if the domain lengths $L^\star$ and $H^\star$ are large enough compared to size of the heated element δ. Indeed, the boundary values should not affect the flow in the central region of the computational domain, that is in the neighbourhood of the plate $Q^\star$.

The system (2-6) is normalized by using as reference variables, the temperature T_1, the size δ of the heat island and a velocity $U_r = \sqrt{g\,\beta\,\delta\,T_1}$. In terms of the non dimensional variable $\mathbf{x} = \mathbf{x}^\star/\delta$, the domain and heated plate respectively read $\Omega = (-L/2, L/2) \times (0, H)$, where $L = L^\star/\delta$ and $H = H^\star/\delta$, and $Q = (-1/2, 1/2)$. The non-dimensional variables

$$\mathbf{u} \,=\, \frac{\mathbf{u}^\star}{U_r}, \;\; \theta \,=\, \frac{T^\star - (T_0 + \alpha_{\rm s}\, y^\star)}{T_1} \;\; \text{and} \;\; p \,=\, \frac{(p^\star + \rho_0\, g\, y^\star)}{\rho_0\, U_r^2} \,-\, \frac{\alpha_s}{2\,\delta\,T_1}\, y^{\star 2} \tag{10}$$

satisfy in Ω and for $t = \frac{U_r}{\delta}\, t^\star > 0$ the following system

$$\frac{\partial \mathbf{u}}{\partial t} - \sqrt{\frac{\rm Pr}{\rm Ra}}\, \Delta \mathbf{u} + \nabla \cdot (\mathbf{u} \otimes \mathbf{u}) + \nabla p \,=\, \theta\, \mathbf{e}_2, \tag{11}$$

$$\nabla \cdot \mathbf{u} \,=\, 0, \tag{12}$$

$$\frac{\partial \theta}{\partial t} - \frac{1}{\sqrt{\rm Ra\, Pr}}\, \Delta \theta + \nabla \cdot (\mathbf{u}\, \theta) \;+\; \alpha\, v = \, 0, \tag{13}$$

where $\alpha = \dfrac{\alpha_s\, \delta^\star}{T_1}$. The non dimensional form of the boundary conditions (7-9) reads

$$\mathbf{u}(\mathbf{x}, t) \,=\, \mathbf{0} \quad \text{on} \;\; \Gamma = \partial\Omega, \tag{14}$$

$$\theta(\mathbf{x}, t) \,=\, 1 \quad \text{on} \;\; \Gamma_Q \,=\, \{\mathbf{x} \in \Gamma;\, y = 0,\, x \in Q\}, \tag{15}$$

$$\theta(\mathbf{x}, t) \,=\, 0 \quad \text{on} \;\; \Gamma \backslash \Gamma_Q. \tag{16}$$

In order to avoid the presence of singularities at the edges of the heated element Q, the temperature boundary condition at the bottom of the domain (15-16) is regularized and is replaced by

$$\theta(\mathbf{x}, t) = \theta_0(x) \quad \text{on} \;\; \Gamma_0 = \Gamma \cap \{x = 0\}, \tag{17}$$

$$\theta(\mathbf{x}, t) \,=\, 0 \qquad \text{on} \;\; \Gamma \backslash \Gamma_0, \tag{18}$$

with

$$\theta_0(x) \,=\, \frac{1}{2}\biggl(1-\tanh\Bigl(\frac{2|x|+1}{2\epsilon}\Bigr)\biggr).$$

The parameter $\epsilon > 0$ was set to $\epsilon = 2.5 \times 10^{-2}$ in the numerical simulations presented in Section 4.

The Prandtl Pr and Rayleigh Ra numbers are defined by

$$\mathrm{Pr} = \frac{\nu}{\kappa} \quad \text{and} \quad \mathrm{Ra} = \frac{g\,\beta\,\delta^3\,T_1}{\nu\kappa}.$$

The Prandtl number is set to $\mathrm{Pr} = 0.71$, which corresponds to air. The system (11-13) depends on two parameters: the Rayleigh number and the non dimensional stratification coefficient α. Note that θ defined by (10) represents the temperature variation from the vertical stratified profile.

3 NUMERICAL APPROXIMATION

3.1 Time discretization

The natural convection problem (11-13) is solved in two steps, which decouple the computation of the temperature and of the velocity-pressure unknowns. A second-order projection scheme[2] is applied to (11,12) in order to compute velocity and pressure. Let us consider that $(\mathbf{u}^j, \theta^j, p^j)$ are known for $j \leq k$, the computation of $(\mathbf{u}^{k+1}, p^{k+1})$ is achieved in two steps. The first (prediction) step consists in

$$\begin{aligned}\frac{\tilde{\mathbf{u}}^{k+1}-\mathbf{u}^k}{\delta t} - \sqrt{\frac{\mathrm{Pr}}{\mathrm{Ra}}}\,\Delta\biggl(\frac{\tilde{\mathbf{u}}^{k+1}+\mathbf{u}^k}{2}\biggr) + \nabla p^k = \,& \frac{1}{2}\left(3\,\theta^k-\theta^{k-1}\right)\mathbf{e}_2 \\ & -\frac{1}{2}\,\nabla\cdot\left(3\,\mathbf{u}^k\otimes\mathbf{u}^k-\mathbf{u}^{k-1}\otimes\mathbf{u}^{k-1}\right), \\ \tilde{\mathbf{u}}^{k+1} \,=\, 0 \quad & \text{on } \Gamma,\end{aligned} \tag{19}$$

and is followed by a projection (correction) step

$$\begin{aligned}&\frac{\mathbf{u}^{k+1}-\tilde{\mathbf{u}}^{k+1}}{\delta t} + \frac{1}{2}\,\nabla(p^{k+1}-p^k) \,=\, 0, \\ &\nabla\cdot\mathbf{u}^{k+1} \,=\, 0, \quad \mathbf{u}^{k+1}\cdot\mathbf{n} \,=\, 0 \quad \text{on } \Gamma.\end{aligned} \tag{20}$$

Finally, the temperature variation θ^{k+1} is solution of

$$\begin{aligned}\frac{\theta^{k+1}-\theta^k}{\delta t} - \frac{1}{\sqrt{\mathrm{Ra}\,\mathrm{Pr}}}\,\Delta\biggl(\frac{\theta^{k+1}+\theta^k}{2}\biggr) \,=& -\frac{1}{2}\,\nabla\cdot\left(3\,\mathbf{u}^k\,\theta^k-\mathbf{u}^{k-1}\,\theta^{k-1}\right) \\ & -\frac{\alpha}{2}\left(3\,v^k-v^{k-1}\right) \\ \theta^{k+1} \,=\, \theta_0(x) \;\text{ on }\; \Gamma_0 \quad \text{and} \quad & \theta^{k+1} \,=\, 0 \;\text{ on }\; \Gamma\backslash\Gamma_0.\end{aligned} \tag{21}$$

3.2 Spatial discretization

Due to the combined effects of the gravity force and of the vertical stratification of the potential temperature, the flow variables are rapidly smoothed with respect to the vertical elevation. Therefore, a uniform mesh of size $h = H/M$ can be applied in the vertical direction, that is $y_j = j\,h$ for $j = 0, \ldots, M$. The aspect ratio L/H of the computational domain Ω being much larger than unity, the mesh is chosen non-uniform in the horizontal direction

$$x_i = \frac{L}{2}\,\varphi(i\,\ell) \quad \text{for} \quad i = 0, \ldots, N,$$

where $\ell = L/N$ and $h = H/M$. The function $\varphi : (0, L) \longrightarrow (-1, 1)$ is defined by

$$\varphi(x) = \frac{2x - L + \gamma_1 \tanh(\gamma_2 x) - \gamma_1 \tanh(\gamma_2 (L - x))}{L + \gamma_1 \tanh(\gamma_2 L)}.$$

The parameters γ_1 and γ_2 are adjusted so that the horizontal mesh sizes being of the order of h in the neighbourhood of the heated element Q.

All the terms in the equations (19,20,21) are discretized in space by second-order centered finite differences. The unknowns are given on a staggered grid[3]. The discrete values of the pressure are located at the center of each mesh cell $K_{ij} = (x_{i-1}, x_i) \times (y_{j-1}, y_j)$, those of the vertical velocity and the temperature are located at the middles of the sides (x_{i-1}, x_i) and those of the horizontal velocity are located at the middles of the sides (y_{j-1}, y_j) as shown on Figure 3.

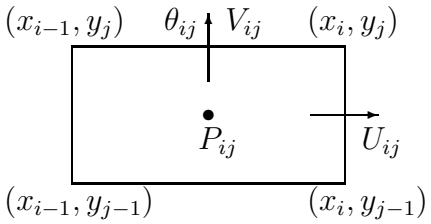

Figure 3: Staggered cell $K_{ij} = (x_{i-1}, x_i) \times (y_{j-1}, y_j)$.

The boundary conditions for v and θ are enforced at mesh points located on the domain boundary. As a consequence, the discretization of $\partial^2\theta/\partial x^2$ at the first mesh point away from the boundary yields modified formulas as

$$\left(\frac{\partial^2\theta}{\partial x^2}\right)_{1,j} \approx \frac{2}{x_{3/2} - x_0}\left(\frac{\theta_{3/2,j} - \theta_{1/2,j}}{x_{3/2} - x_{1/2}} - \frac{\theta_{1/2,j} - \theta_{0,j}}{x_{1/2} - x_0}\right)$$

where $x_{i+1/2} = \frac{x_i + x_{i+1}}{2}$ for $i = 0, \ldots, N-1$. A similar formula is applied at the last inner point in the horizontal direction, that is $x_{N-1/2}$. In the vertical direction, the use of

second-order centered formula and of uniform mesh points allows us to apply a discrete Fourier transform[4] leading to a set of independent and symmetric tridiagonal systems which can be efficiently solved with the $\mathrm{LDL}^{\mathrm{T}}$ algorithm.

The conditions for u on the vertical boundaries are enforced at mesh points x_0 and x_N. At the top and bottom boundaries, *ghost* points $y_{-1/2} = -h_1/2$ and $y_{M+1/2} = H + h_M/2$ are introduced. Values for u at these *ghost* points are obtained by applying second-order extrapolation and by simultaneously enforcing the boundary conditions at y_0 and y_M. The discretization of $\partial^2/\partial y^2$ on the sequence of mesh points $y_{1/2}, \ldots, y_{M-1/2}$ with second-order centered finite difference also yields a discrete operator which can be easily diagonalized by applying a discrete Fourier transform[4].

3.3 A *truncated* temperature equation

In order to obtain accurate solutions, the numerical simulation of (19-21) has to be achieved in long domains with an aspect ratio $L/H \gg 1$. Indeed, solutions of (19-21) have a slow decay with respect to the horizontal distance from the heated plate Q. If L is not sufficiently large, an artificial boundary layer develops at the vertical boundaries $x = \pm L/2$ whose effect is to deteriorate the accuracy of the computed temperature variation in the central area of the domain. In order to overcome this difficulty, we modify the temperature variation equation (13) as follows

$$\frac{\partial \theta}{\partial t} - \frac{1}{\sqrt{\mathrm{Ra}\,\mathrm{Pr}}}\,\Delta\theta + \psi(x)\left(\nabla\cdot(\mathbf{u}\,\theta) + \alpha\, v\right) \;=\; 0, \tag{22}$$

where

$$\psi(x) \;=\; \exp - \left(\frac{|2x - L|}{\sigma L}\right)^p,\ \sigma \in (0,1).$$

As values for the parameters, $\sigma = 0.9375$ and $p = 8$ were used in the numerical simulations presented hereafter.

Equation (22) is supplemented with the boundary conditions (17) and (18). The net effect of the *horizontal filtering* function ψ is to reduce the convective terms in an area close to the domain boundaries namely for $|x| \geq \sigma\, L$. This numerical technique is similar to the so-called *sponge-layer* technique used for the numerical simulation of compressible turbulence[5,6]. The efficiency of the *truncated* equation (22) is investigated in the next section through the numerical simulations of stationary and time periodic solutions of (11-13).

4 NUMERICAL RESULTS

4.1 Stationary solutions

Stationary solutions are first computed at $\mathrm{Ra} = 10^5$. The resolution in the neighbourhood of the heated plate Q is set to $h = 1/32$, that is $32 \times H$ uniform mesh points are used in the vertical direction. In order to obtain an accurate reference solution for this

resolution, numerical simulations of system (19-21) are performed for increasing values of the domain length L in the range $(160, 6200)$. The value $H = 6$ for the domain height is sufficient to obtain accurate solutions at this resolution and Rayleigh number. A grid of 14000×192 mesh points is used for the limit case $L = 6200$.

In order to check the accuracy of the simulated solutions, we compare the values of the minimum of the temperature variation $\min \theta_L$ obtained for different computational domains $(0, L) \times (0, 6)$ with $L \in [160, 6200]$. Figure 4, representing the relative accuracy

$$\frac{|\min \theta_L - \min \theta_{6200}|}{|\min \theta_{6200}|},$$

shows that $L \geq 1600$ is necessary in order to obtain a h^2 accurate approximation of the reference value $\min \theta_{6200} = -0.17156$ which is reached along the $x = 0$ axis at elevation $y = 0.85063$. When using the *truncated* temperature equation (22) instead of (21), a h^2 accurate approximation, namely $-.171521$, is obtained for $L = 400$ on a grid of 2600×192 points. This result demonstrates the efficiency of the *truncated* temperature equation which allows to significantly reduce the computational domain length.

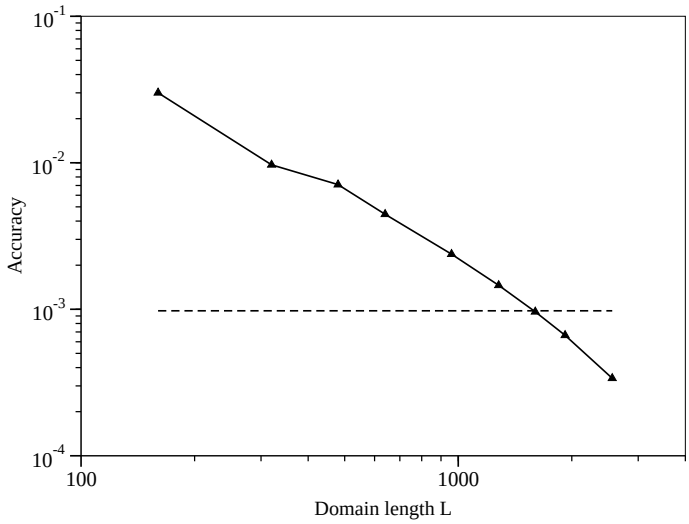

Figure 4: Accuracy of the stationary solution at $\mathrm{Ra} = 10^5$ as a function of the domain length L. The dashed line is used to indicate the expected accuracy $h^2 = 1/32^2$.

A stationary solution is also obtained at $\mathrm{Ra} = 2.5 \times 10^5$. On Figure 5, the profile of the temperature variation at the center of the heated plate is shown for $\mathrm{Ra} = 10^5$ and 2.5×10^5. As shown on Figure 6, stationary solutions are symmetric with respect to the horizontal distance x from the center of the heated plate. The increase of the Rayleigh number induces lower values for $\min \theta(0, y)$ and for the elevation where this minimum is reached:

the flow is pushed down. This phenomenon participates to the loss of symmetry of the solutions at larger Rayleigh numbers and to the appearance of time evolutive solutions.

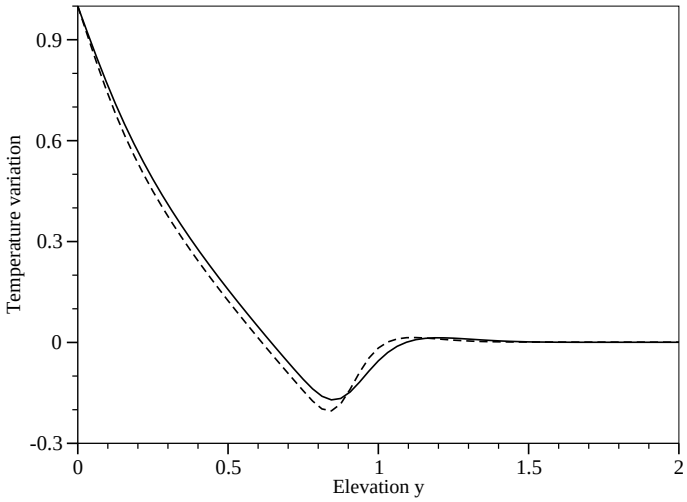

Figure 5: Profile of the temperature variation θ at the center of the heat island, *i.e.* $\theta(0, y)$, for $\mathrm{Ra} = 10^5$ (solid line) $\mathrm{Ra} = 2.5 \times 10^5$ (dashed line).

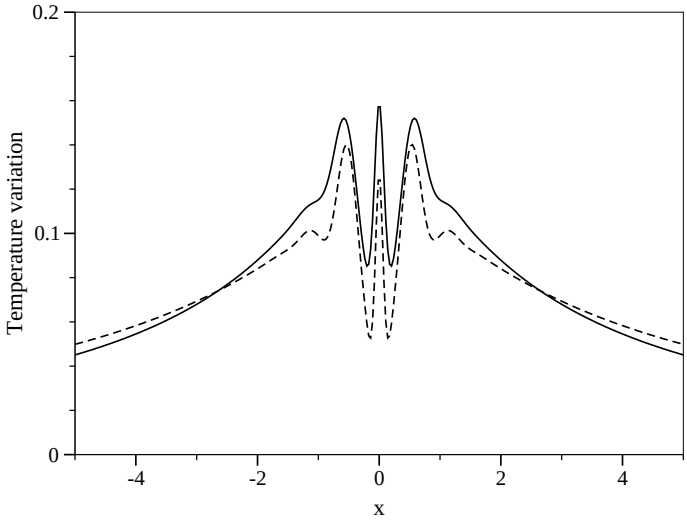

Figure 6: Profile of the temperature variation θ at the elevation $y = 0.5$, *i.e.* $\theta(x, 0.5)$, for $\mathrm{Ra} = 10^5$ (solid line) $\mathrm{Ra} = 2.5 \times 10^5$ (dashed line).

4.2 Time periodic solutions

At Ra $= 10^6$ a time periodic solution is captured. Numerical simulations with the *truncated* temperature equation have been performed with $L = 320$, 400 and 640 in order to check the accuracy and validity of the results. Characteristic values of the time signal observed at two different points in the computational domain, namely $\mathbf{x}_1 = (-0.5, 0.5)$ and $\mathbf{x}_2 = (0, 0.5)$, are reported in Table 1. The differences between the values obtained for $L = 400$ and 640 are smaller than h^2 indicating that convergence with respect to the domain length is achieved. Clearly, $L = 320$ is not large enough to obtain accurate results. The time periodic signal $\theta(\mathbf{x}_2, t)$ is shown on Figure 7.

A time periodic solution is also found at Ra $= 5 \times 10^5$ as shown on Figure 8. The value of the time period is 7.375 and the temperature at point $\mathbf{x}_2$ oscillates between a minimum value of 0.09225 and a maximum value of 0.09974.

This results obtained at the moderate resolution $h = 1/32$ indicate that a first Hopf bifurcation for the heat island problem studied in this paper occurs for a Rayleigh number lying between 2.5×10^5 and 5×10^5.

	$L = 320$	$L = 400$	$L = 640$
Time period	14.258	14.265	14.265
$\min \theta(\mathbf{x}_1, t)$	0.07504	0.07443	0.07456
$\max \theta(\mathbf{x}_1, t)$	0.11974	0.11908	0.11920
$\min \theta(\mathbf{x}_2, t)$	0.02421	0.02394	0.02399
$\max \theta(\mathbf{x}_2, t)$	0.07871	0.07847	0.07851

Table 1: Characteristic values of the temporal signal $\theta(\mathbf{x}, t)$, for $t > 10000$, at points $\mathbf{x}_1 = (-0.5, 0.5)$ and $\mathbf{x}_2 = (0, 0.5)$ and at Ra $= 10^6$.

5 CONCLUSIONS

Two dimensional numerical simulations of flows induced by a heat island perturbation in an unbounded domain have been performed. The direct computations of the stationary solution at Ra $= 10^5$ and with a resolution $h = 1/32$ in *large* domains for L varying from 160 through 6200 have been used as references in order to show the efficiency of the *truncated* temperature equation. This numerical procedure allowing to significantly reduce the domain length is applied to the numerical simulation of stationary solutions at Ra $= 2.5 \times 10^5$. Time periodic solutions have been found for Ra $= 5 \times 10^5$ and Ra $= 10^6$ indicating that the first Hopf bifurcation occurs for Ra $\in (2.5 \times 10^5, 5 \times 10^5)$. Preliminary results have been reported here and further investigations are needed in order to accurately detect the critical Rayleigh number corresponding to this bifurcation.

ACKNOWLEDGMENTS

The numerical simulations presented in this work were done on the cluster of IBM Power 4 computers of the Supercomputing Center IDRIS of CNRS (Orsay, France). The code

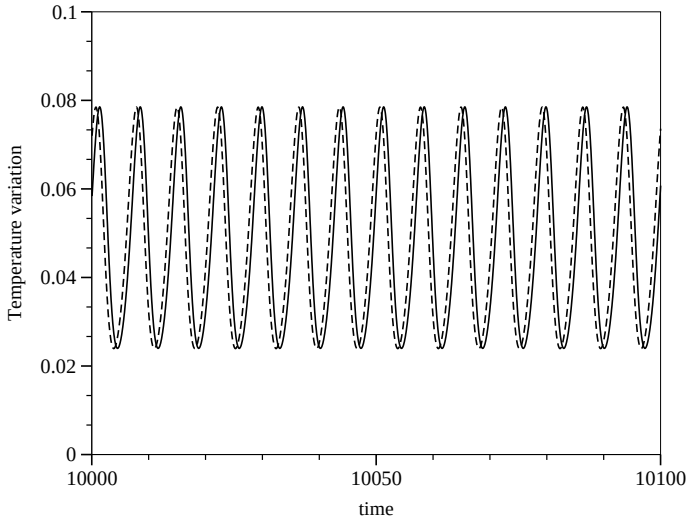

Figure 7: Time history of the temperature variation $\theta(\mathbf{x}_2, t)$ obtained at Ra $= 10^6$ and for $L = 400$ (dashed line) and $L = 640$ (solid line).

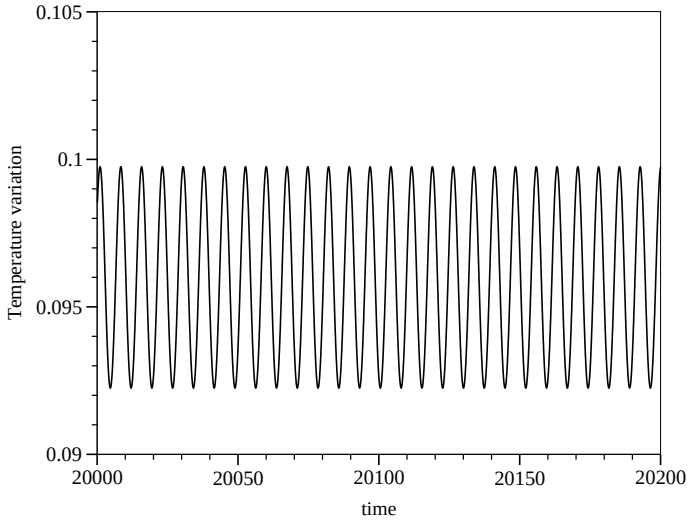

Figure 8: Time history of the temperature variation $\theta(\mathbf{x}_2, t)$ obtained at Ra $= 5 \times 10^5$ and for $L = 400$.

was parallelized using implicit communications (OPENMP). The number of processors used simultaneously varies from 4 to 10 depending on the number of mesh points.

REFERENCES

[1] Y. Delage and P.A. Taylor. Numerical studies of heat island circulation. *Boundary-Layer Meteorology*, **1**, 201–226, 1970.

[2] J. Van Kan. A second-order accurate pressure-correction scheme for viscous incompressible flow. *SIAM J. Sci. Stat. Comput.* 1986 ; **7**(3) : 870–891.

[3] F.H. Harlow and J.E. Welch. Numerical calculation of time-dependent viscous incompressible flow of fluid with free surface. *Physics of Fluids*, **8**(12) : 2182–2189, 1965.

[4] U. Schumann and R.A. Sweet. Fast Fourier transforms for direct solution of Poisson's equation with staggered boundary conditions. *J. Comp. Phys.* 1988 ; **75** : 123–137.

[5] D. Givoli. Non-reflecting boundary conditions. *J. Comp. Phys.* 1991 ; **94** : 1–29.

[6] M. Israeli and S.A. Orszag. Approximation of radiation boundary conditions. *J. Comp. Phys.* 1981 ; **41** : 115–135.